Elucidating the Binding Mode between Heparin and Inflammatory Cytokines by Molecular Modeling

Mingjia Yu,*[a] Tianji Zhang,[b] Jin-ping Li,[a, c] and Yingxia Tan*[d]

Heparan sulfate (HS) interacts with a broad spectrum of inflammatory cytokines, thereby modulating their biological activities. It is believed that there is a structural-functional correlation between each protein and sugar sequences in the HS polysaccharides, however, the information in this regard is limited. In this study, we compared the binding of four inflammatory cytokines (CCL8, IL-1beta, IL-2 and IL-6) to immobilized heparin by an SPR analysis. To define the molecular base of the binding, we used a heparin pentasaccharide as representative structure to dock into the 3D-molecular structure of the cytokines. The results show a discrepancy in K_D values obtained by SPR analysis and theoretical calculation, pointing to the importance to apply more than one method when describing affinity between proteins and HS. By cluster analysis of the complex formed between the pentasaccharide and cytokines, we have identified several groups in heparin forming strong hydrogen bonds with all four cytokines, which is a significant finding. This molecular and conformational information should be valuable for rational design of HS/heparin-mimetics to interfere cytokine-HS interactions.

1. Introduction

Heparan sulfate denotes a group of negatively charged polysaccharides ubiquitously expressed on the cell surface and the extracellular matrix (ECM),[1] regulating a broad spectrum of biological and pathophysiological activities. The functions of HS are transmitted, mainly, through interaction with proteins, for example, cytokines and chemokines.[2] The multi-functional properties of HS owe to its structural diversity, such as distinctive molecular structures which are expressed on the same cell surface, binding to different protein ligands for distinct functions. The complexity and variety of HS structures are generated through a complex biosynthesis process dictated by a remarkable regulatory machinery, enabling a stringent structure-function correlation for a given circumstance.[3]

Inflammatory cytokines are signaling molecules secreted predominantly from immune cells, for example, T helper cells and macrophages, promoting inflammatory reactions. The cytokines act on the target cells through binding to receptors on the cell surface. An array of inflammatory cytokines can be activated by HS,[4] such as microphage inflammatory protein (MIP-1α), monocyte chemoattractant protein 1 (MCP1/CCL2),[5] monocyte chemoattractant protein 2 (MCP2/CCL8)[6] and several interleukins.[7] On the target cell surface, HS binds to the cytokines, serving as a co-receptor. In the extracellular matrix, HS functions as a storage for secreted cytokines and modulates their activities. A HS polysaccharide chain is generally composed of about 100 sugar units that are variably sulfated and may harbor several binding sequences for different cytokines. Thus, to illustrate the molecular interaction mode between a given protein and HS, it is of importance to understand the functional implications.[8]

Heparin is an anticoagulant drug widely used for prevention and treatment of thrombosis. Clinical applications observed, apart from its anticoagulation activity, beneficial 'side effects' of heparin, one of which is attenuation of inflammation. Indeed, our retrospective study found that application of low molecular weight heparin (LMWH) significantly reduced the IL-6 level in the plasma of severely ill COVID-19 patients.[9] These functions of heparin are most likely due to interferences arising from the interactions between HS and inflammatory cytokines, because heparin and HS polysaccharides are synthesized by the same process and share high structural similarity. Based on the structural similarity, heparin is generally capable of binding to all HS-binding proteins, disrupting their functions. Such effects of heparin are of potential value for expanded applications. To avoid the potential risk of bleeding, heparin has been chemically modified to abolish its anticoagulation activity, resulting in non-anticoagulant heparin.[10] An alternative approach is to produce heparin/HS-mimetics. A few species of such heparin/HS-mimetics have been explored for anticancer activity.[11]

To develop heparin/HS-mimetics for interfering with the HS-protein interaction, one challenge is to elucidate the HS

[a] Dr. M. Yu, Prof. Dr. J.-p. Li
Beijing Advanced Innovation Centre for Soft Matter Science and Engineering
Beijing University of Chemical Technology, Beijing 100029 (China)
E-mail: 2019750009@mail.buct.edu.cn
[b] Dr. T. Zhang
Division of Chemistry and Analytical Science
National Institute of Metrology, Beijing 100029 (China)
[c] Prof. Dr. J.-p. Li
Department of Medical Biochemistry and Microbiology
University of Uppsala, Uppsala (Sweden)
[d] Prof. Dr. Y. Tan
Department of Stem Cell and Regenerative Medicine
Institute of Health Service and Transfusion Medicine, Beijing 100000 (China)
E-mail: tanhu333@126.com

Supporting information for this article is available on the WWW under https://doi.org/10.1002/open.202100135

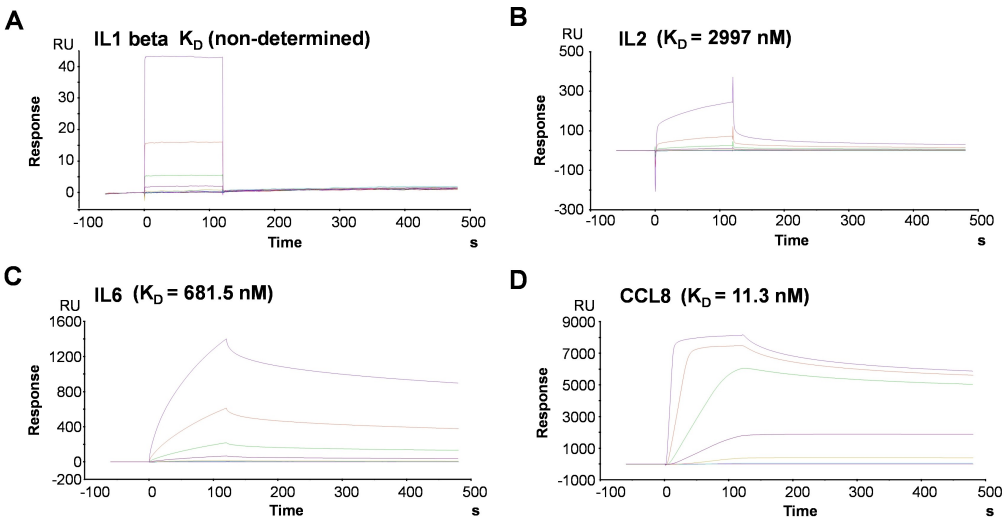

Figure 1. SPR sensorgrams showing the interactions between immobilized heparin and the cytokines. The K_D value of each cytokine is presented on top of the corresponding sensorgram.

sequences specifically binding to the target proteins. In this work, we aimed at defining the structure-function correlation of heparin (as well as heparin/HS-mimetics) with four inflammatory cytokines, CCL8, IL-1beta, IL-2 and IL-6. Surface Plasmon Resonance (SPR) analysis showed a differential affinity of the cytokines in binding to immobilized heparin. The interaction mode was analyzed by molecular modeling. The results demonstrate that the combination of biochemical and modeling analysis could contribute to rational design of heparin/HS-mimetics for the purpose of modulating the activities of cytokines as well as other HS-binding proteins.

2. Results and Discussion

2.1. Surface Plasmon Resonance (SPR) Analysis of the Cytokines Binding to Immobilized Heparin

To confirm the immobilization of the biotinylated heparin onto the SA gold sensor chip surface, we utilized FGF2 as a well characterized heparin-binding protein to test the binding capacity. The serial diluted FGF2 samples (from high to low concentration) were injected into the channel at a constant flow of 30 $\mu L\,min^{-1}$. The changes in refractive index caused by molecular interactions at the sensor surface were monitored and recorded as response unit. Calculation of the dissociation constant showed a K_D value of 5.79 nM (Figure S2, Supporting Information), which is in good agreement with previous report,[12] indicating a good reactivity of the immobilized heparin. Using the same setting, IL-1beta, IL-2, IL-6 and CCL8 were sequentially analyzed. The chip was washed with HBS-P for 360 s and regenerated with 50 mM NaOH for 10 s between each run. The sensorgrams of the analysis are shown in Figure 1. The collected data are calculated by the software (GraphPad, La Jolla, CA) the SPR instrument is equipped with. Comparison of the dissociation constants revealed a dramatic difference between the cytokines in binding to heparin. IL-1beta did not bind to the immobilized heparin, while CCL8 displayed an affinity as high as FGF2.

2.2. Analysis of Heparin-Cytokine Interactions by Molecular Modeling

To explore the mechanistic basis for the differential affinity between the cytokines and heparin, we analyzed the interactions by molecular modeling using the AutoDock VINA and molecular dynamics (MD) in the YASARA program[13] and APBS (Adaptive Poisson-Boltzmann Solver) Electrostatics[14] Plugin in PyMOL (The PyMOL Molecular Graphics System, Version 2.0 Schrödinger, LLC). The structural information of the cytokines was obtained from the PDB as described in the Experimental Section. To reduce the complexity of the macromolecular heparin, we used a pentasaccharide sequence (Figure 2) that was docked into the molecular structures of the four cytokines, respectively. The results show formation of an interaction complex between each of the cytokines with the pentasaccharide (Figure 3). Calculation of binding free energy and predicted K_D values (Table 1) show a higher affinity between CCL8 and the pentasaccharide, which is in agreement with the result obtained by SPR. This is likely due to the basic amino acids at the surface (blue), which provide a strong positive electrostatic environment, forming salt bridge interactions with the negatively

Table 1. The binding free energies ($kcal\,mol^{-1}$) and predicted K_D values (μM) between the heparin pentasaccharide and cytokines.

Receptor proteins	Binding free energies [$kcal\,mol^{-1}$]	K_D [μM]
IL-1beta	−5.90	47.7
IL-2	−5.97	42.3
IL-6	−6.15	30.8
CCL8	−6.42	19.8

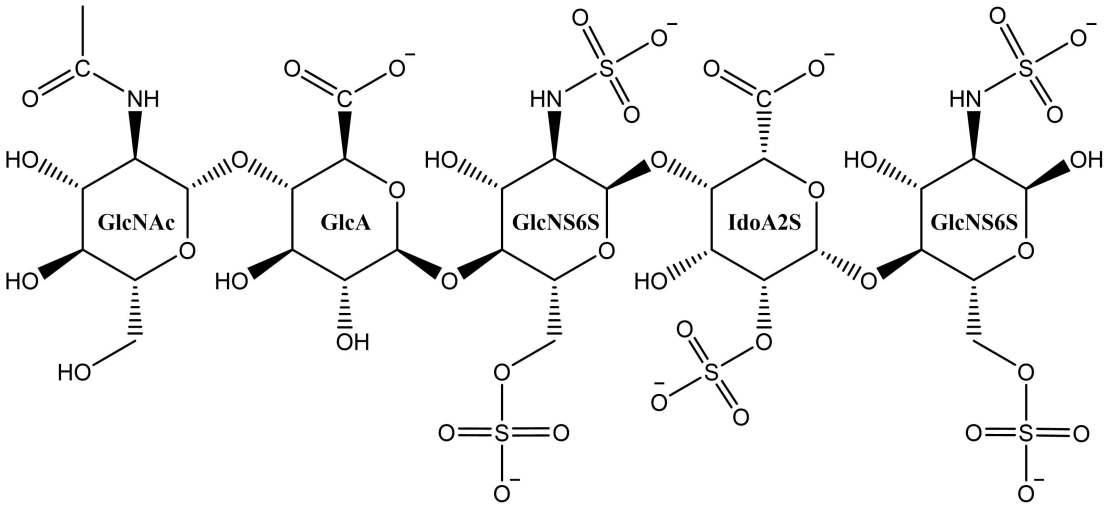

Figure 2. Chemical structure of the heparin pentasaccharide sequence used in this study. GlcNAc (N-acetylated glucosamine); GlcA (glucuronic acid, $^4C_1$); GlcNS6S (N- and 6-O-sulfated glucosamine); IdoA2S (2-O-sulfated iduronic acid, $^1C_4$)

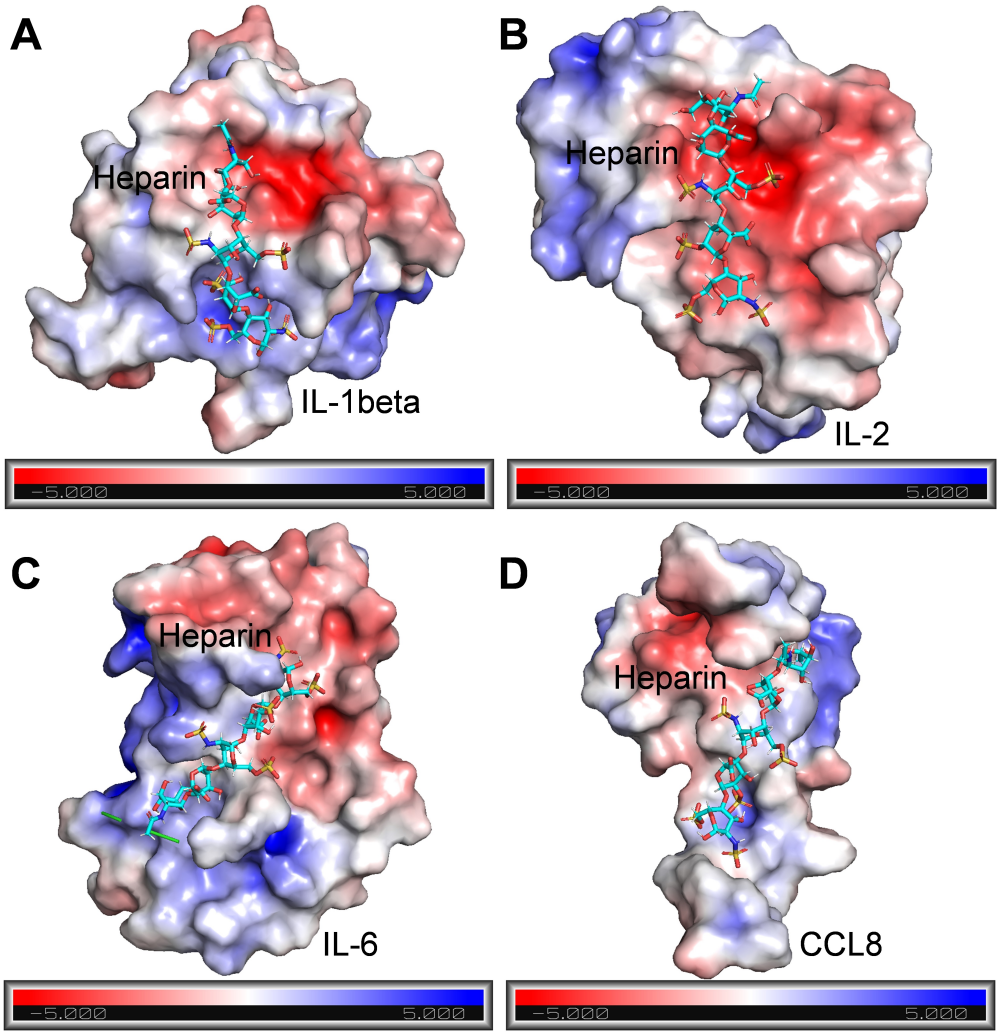

Figure 3. Interaction complex between each of the cytokines with the heparin pentasaccharide. The electrostatic surface rendering maps of **(A)** IL-1beta (PDB ID: 1ITB), **(B)** IL-2 (PDB ID: 6YE3), **(C)** IL-6 (PDB ID: 1ALU) and **(D)** CCL8 (PDB ID: 1ESR) docked with the pentasaccharide are shown. Blue colored surfaces indicate electropositive and red surfaces indicate electronegative patches. The pentasaccharide is displayed using the standard licorice format.

charged groups in heparin. In contrast, the pentasaccharide was docked into a patch of acidic amino acids in IL-2, indicating that, while salt-bridge interactions do not contribute to the interaction between IL-2 and the pentasaccharide, weaker hydrogen-bond interactions do.

To elucidate the binding modes, we examined the docking complexes through a 2D diagram (Figure 4). The amino acid residues (Thr10, Ile9, Asn33, Thr32, Arg30, Ile31, Tyr28, Asp68) on the surface of CCL8 (Figure 4D and Table S4) interact with both N- and 6-O-sulfo groups of GlcNS6S, 2-O-sulfo, as well as the hydroxy groups of IdoA2S, GlcA and GlcNAc by hydrogen bonds. In comparison, the negatively charged amino acid residues (Asp142 and Asp145) of IL-1beta form hydrogen bonds with hydroxy groups of GlcNAc (Figure 4B), while the negatively charged amino acids of Glu55, Glu56, Glu57 and Glu63 on IL-2 enabled formation of hydrogen bonds with N- and 6-O-sulfo groups of GlcNS6S and hydroxy groups of IdoA2S and GlcNAc (Figure 4A). Notably, the negatively charged groups on amino acid residues of Ser13 (IL-1beta), Glu55, Glu56 and Glu57 (IL-2) and Glu93 (IL-6) form negative-negative ionic interactions with hydroxy groups of GlcA, 6-O-sulfo groups of GlcNS6S, which may inactivate the anionic attractivity of the sulfo- and carboxyl groups in the pentasaccharide.

2.3. Structural Dependence of IL-6 Interaction with Sulfated Polysaccharides

To further probe the selectivity of cytokine binding to polysaccharides, we applied a different approach by immobilization of a protein (IL-6) on the Series S Sensor Chip CM5 to which binding of the four polysaccharides were analyzed. Serial dilutions of heparin at the concentration of 500–15.625 μM, OD-heparin (O-desulfated heparin) at the concentration of 100–12.5 μM, NS-K5 (N-sulfated K5 polysaccharide) at the concentration of 20–1.25 μM and HS (heparan sulfate) at the concentration of 200–6.25 μM were injected at a constant flow of 30 μL min^{-1}. SPR analysis resulted in a low RU recording for all samples, indicating an overall low binding of the polysaccharides to the immobilized IL-6. Nevertheless, calculation of K_D values revealed differences in binding affinity of the polysaccharides. OD-heparin and NS-K5 had a slightly higher affinity than heparin in binding to IL-6, while the native HS displayed the lowest affinity to IL-6 (Figure S3).

To find out whether there is indeed a difference in binding of the polysaccharides to IL-6, we analyzed the interaction mode by molecular modeling using a pentasaccharide structure of each polysaccharide (Figure 5) including heparin (Figure 2). Docking of the oligosaccharides into the IL-6 3D molecular structure resulted in complex formation (Figure 6), indicating binding of each pentasaccharide to IL-6. Molecular docking

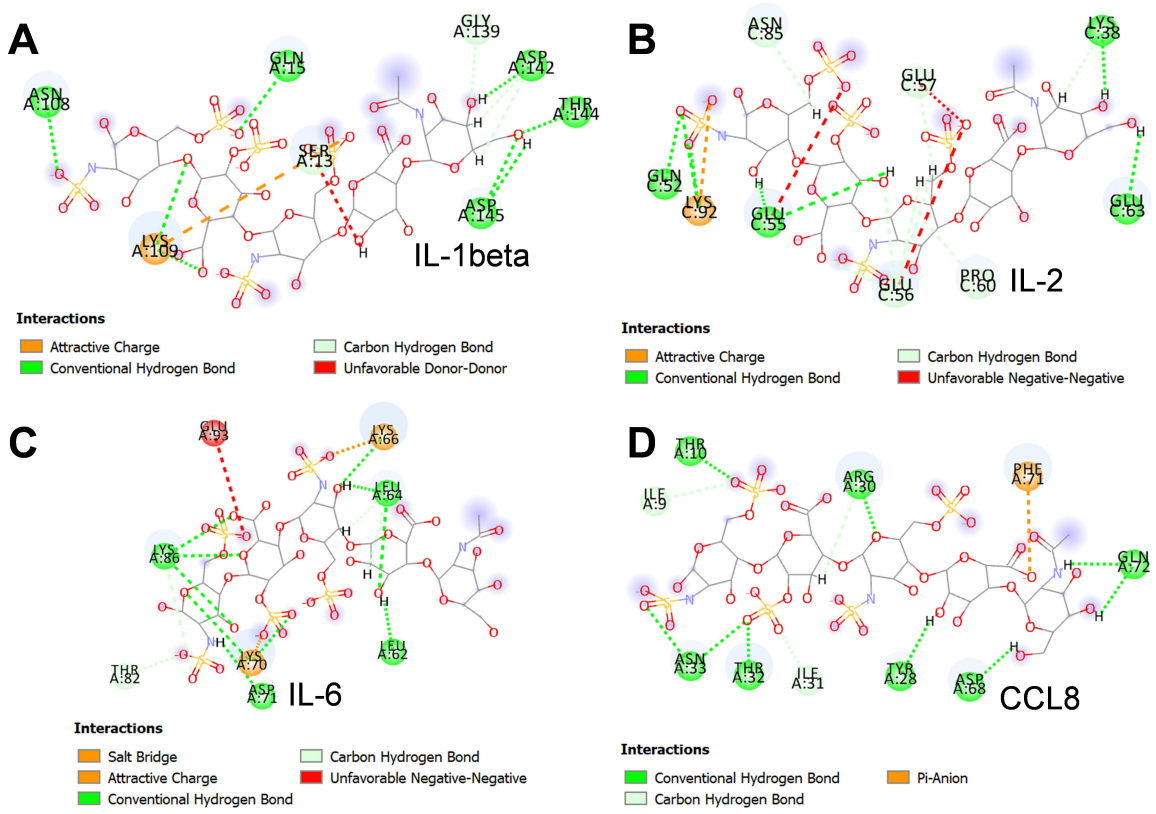

Figure 4. 2D diagrams showing the interaction mode between the cytokines and heparin pentasaccharide. The amino acid residues interacting with the pentasaccharide are highlighted by colored dots. The interaction groups are featured by colored lines which are explained under each diagram. The round shadows indicate distant spatial location. The 2D diagrams were generated by Discovery Studio v. 4.5.

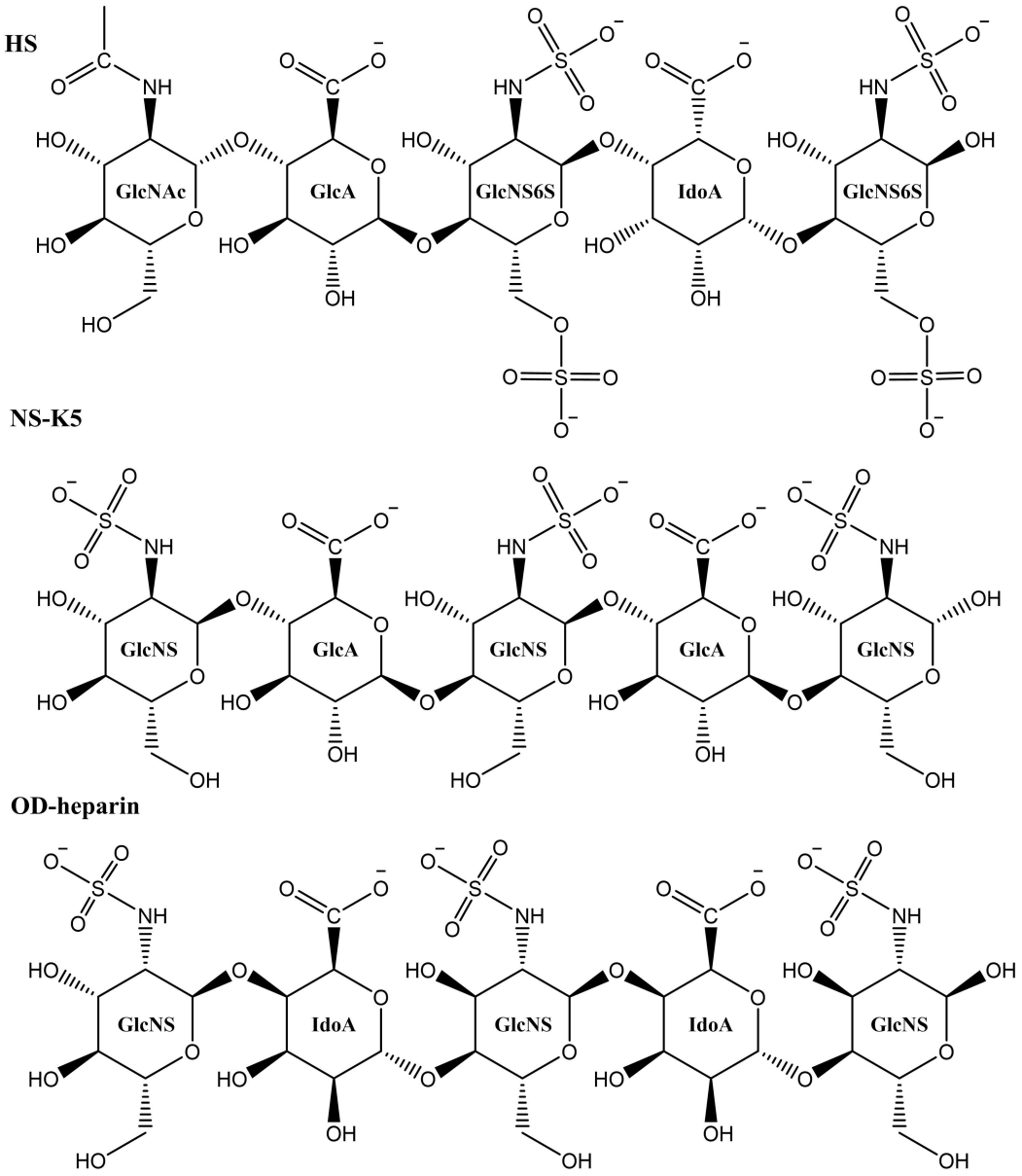

Figure 5. The chemical structures of pentasaccharide sequences of the polysaccharides used in this study. GlcNAc (N-acetylated glucosamine); GlcA (glucuronic acid, $^4C_1$); GlcNS6S (N- and 6-O-sulfated glucosamine); IdoA (iduronic acid, $^1C_4$).

calculation by Autodock Vina in YASARA program (version 19.5.23), revealed differences in the binding free energy and predicted K_D values of the pentasaccharides towards IL-6 (Table 2).

Overlay of the complexes shows that the pentasaccharides of heparin/NS-K5/HS (green/cyan/light blue) docked into the domain of B and D helixes in IL-6, while OD-heparin (pink) docked into the domain of B and C helixes in IL-6 (Figure 6, panel B), shifted by ≈16 Å away from the site where the other three oligosaccharides bound. From an overhead view of the overlapping complexes (Figure 6, panel C), HS appeared having a loose reducing end (shown in red circle) on the outer side of electron density map of IL-6, having no interaction with IL-6, which may lead to its weaker interaction with IL-6. The 2D diagrams further illustrate the different mode of interactions between IL-6 and the pentasaccharides (Figure 7). The distinctive binding site of OD-heparin from the other three pentasaccharides may lie beside the middle domain of B and head domain of C helixes in IL-6, where the binding site might be the closest position of these pentasaccharides binding to IL-6.

Table 2. The binding free energies (kcal mol^{-1}) and predicted K_D values (μM) between IL-6 and the 4 pentasaccharides.

Receptor proteins	Binding free energies [kcal mol^{-1}l]	K_D [μM]
Heparin	−6.15	30.8
NS-K5	−6.40	20.3
HS	−5.73	62.8
OD-heparin	−6.70	12.2

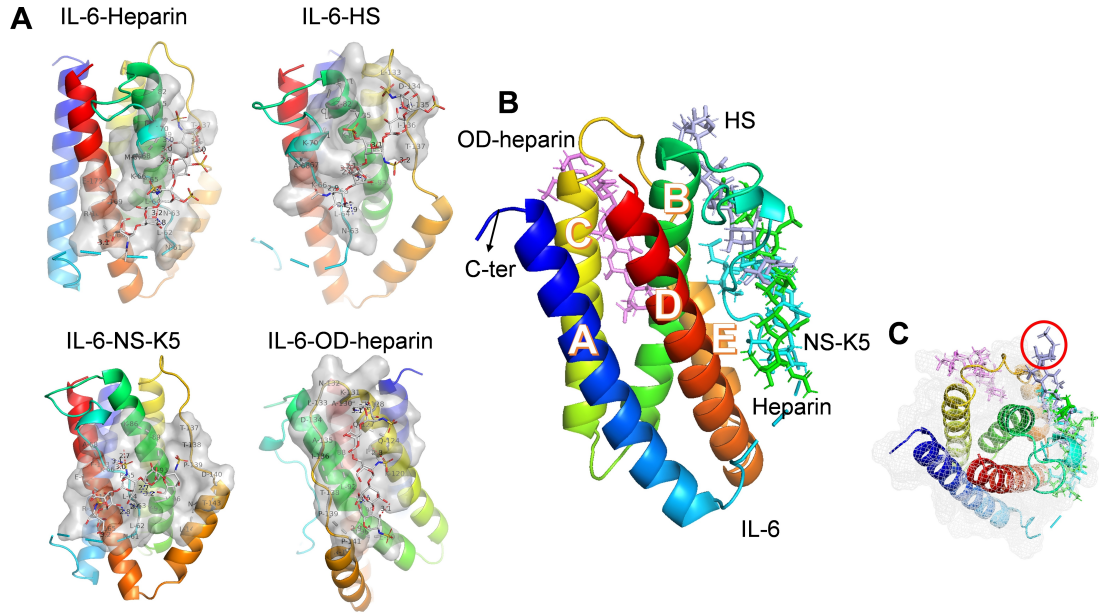

Figure 6. (A) Complex formed between IL-6 and the 4 pentaccharides; **(B)** Superposition of the complexes: heparin,[23] HS (light blue), NS-K5 (cyan) and OD-heparin (pink). Ribbon representation of the IL-6 crystal structure, the four main helices labeled as A, B, C and D. The extra helix in the final long loop is labeled E. **(C)** Overhead view of **B**, grey mesh represents the electron density map of IL-6 drawn by PyMOL. The red circle highlights the loose reducing end of HS.

2.4. Common Features of Heparin in Interaction with Cytokines

Since all four cytokines showed interaction with the heparin pentasaccharide, we wanted to examine whether there are specific groups of heparin contributing to the interactions with the cytokines. By cluster analysis, we identified the key chemical groups on heparin that form strong hydrogen bonds with amino acid residues of all four proteins (Figure 8). The OH at C4 (nr. 2) of GlcNAc, OH at C2 (nr. 35) of GlcA, OH at C3 (nr. 14) of GlcNS6S and O at 2-O-sulfo (nr. 37) of IdoA2S displayed the strongest intensity, indicating higher frequency in interaction with the proteins. The moderate intensity groups of OH at C6 (nr. 8) of GlcNAc, OH at C3 (nr. 33) of GlcA, OH at C3 (nr. 13) and O at carbonyl (nr. 11) of IdoA2S, O at 6-O-sulfo (nr. 16) and O at N-sulfo (nr. 36) of GlcNS6S have a medium interactivity with the proteins, while the light-colored groups are only reactive towards a specific amino acid of in one of the proteins. The hydrogen bonds formed between heparin and each of the protein ligands are listed in Table S1–S7.

To justify whether the models constructed from molecular docking are reliable, the molecular dynamics (MD) simulations of each cytokine with a pentasaccharide heparin bound were performed. The RMSD values of the structures aligned by PyMOL including the last structure of IL-1beta + Heparin/IL-2 + Heparin/IL-6 + Heparin/IL-6 + HS/CCL8 + Heparin/IL-6 + NS-K5/IL-6 + OD-heparin obtained from the MD and the complex of IL-1beta + Heparin/IL-2 + Heparin/IL-6 + Heparin/IL-6 + HS/CCL8 + Heparin/IL-6 + NS-K5/IL-6 + OD-heparin obtained from molecular docking complexes are small (Figure S4), which means that the structural variance is minor and the structures of complexes obtained from molecular docking are reliable.

3. Conclusion

Heparan sulfate plays vital roles in animal development and homeostasis through modulating biological functions of a large number of growth factors and cytokines.[15] Biochemical analysis identified hundreds of proteins interacting with HS (and heparin due to structural similarity);[16] however, information on the binding mode between the proteins and HS/heparin is barely available. In this study, we examined the molecular interactions of heparin with four inflammatory cytokines (CCL8, IL-1beta, IL-2 and IL-6) that are known binding to HS by molecular docking[17] in combination with the conventional SPR analysis.

Comparing the K_D values calculated from the molecular docking and SPR analysis finds a dramatic difference, indicating the two methods are not directly comparable for assessment of apparent affinity. This discrepancy between the two methods may be caused by several factors. The SPR used full-length heparin that is immobilized on a surface, while the molecular docking used a pentasaccharide that is freely movable in the system. Nevertheless, CCL8 displayed the highest affinity and IL-1beta had the lowest affinity by both methods. The dramatic discrepancy in the binding affinity between IL-6 and heparin obtained by immobilization of heparin (K_D = 681.5 nM) and immobilization of IL-6 (K_D = 696 μM) is of worth noting. Most of the reported biochemical analysis for protein-sugar binding (including heparin, heparin-mimetics and glycosaminoglycans) uses the method to immobilize sugars, including glycan-arrays[18] and SPR analysis.[19] Since the immobilization may affect the reactivity and interaction mode, different methods, including molecular modelling,[20] should be applied when define binding affinity between a given protein and heparin/HS or glycosaminoglycans. A significant point revealed by molec-

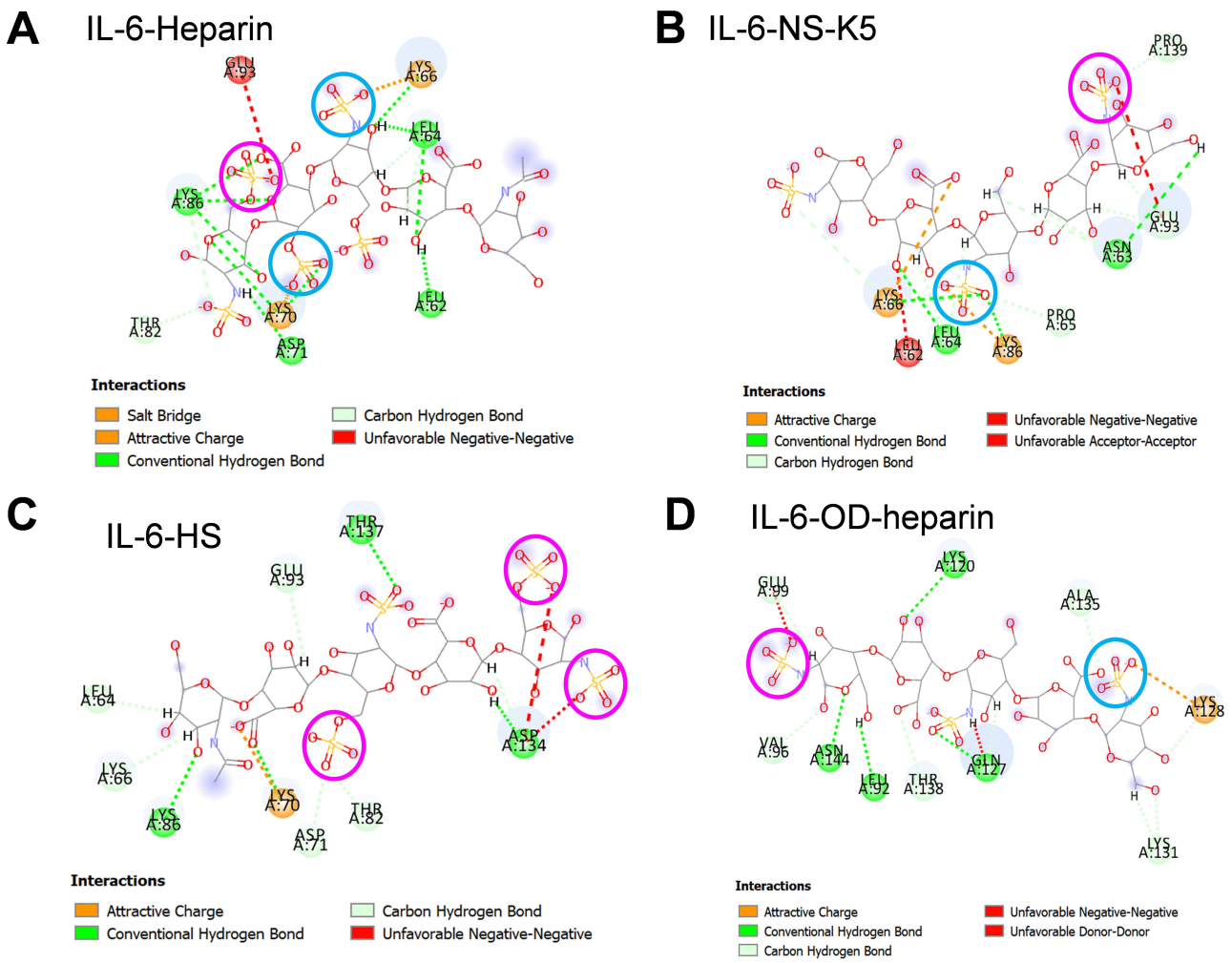

Figure 7. 2D diagrams of the interaction between IL-6 and the pentasaccharides as indicated. The interaction groups are featured by colored lines explained under each diagram. Blue circles represent sulfo group-basic amino acid interaction; Pink circles represent sulfo group-acidic amino acid interaction. The round shadows indicate distant spatial location. The 2D diagrams were generated by Discovery studio v4.5.

ular modeling is that the positively charged amino acids (Lys66, Lys70 and Lys86) on the surface of IL-6 formed hydrogen bonds primarily with the N- and 6-O-sulfo groups of GlcNS6S and 2-O-sulfo group of IdoA2S in heparin, instead of salt bridges as observed for CCL8. This is due to the negative-negative ionic interactions between Glu93 in IL-6 and 6-O-sulfo group of GlcNS6S in the pentasaccharide, leading to losing or weakening of the binding between positively charged amino acids and the negative groups in heparin.

One unexpected finding by overlay of the IL-6 complexes is that the pentasaccharide of HS, the theoretical endogenous molecule, displayed the lowest affinity, while the pentasaccharide of OD-heparin showed the highest affinity, though it binds on a negative electrostatic environment of IL-6 surface (Figure S5). OD-heparin and NS-K5 carry the same number of O-sulfo groups, but NS-K5 has two glucuronic acids (GlcA), while OD-heparin has two iduronic acids (IdoA). Most likely, the conformation of IdoAs renders the sugar fitting well with the shape complementarity of IL-6 on a different site from where the other three pentasaccharides bind. Regardless, none of the pentasaccharides binds to the receptor binding site on IL-6,[21] indicating a potential risk that these structures of heparin mimetics may not interfere with the interaction of IL-6 with its receptor (Figure 6; panel B).

A last important finding consists of the identification of active groups in heparin. By cluster analysis to compare the binding between the heparin pentasaccharide with the four cytokines, we localized the chemical groups in heparin that have a high frequency to interact with the proteins by forming hydrogen bonds. This information is valuable for rational design of HS/heparin-mimetics to interfere with the HS-protein interactions. As an implication for the chemical synthesis of non-sugar-based HS/heparin-mimetics, these reactive groups might be included in a given organic molecule.

In consideration of the important pathophysiological functions of HS in diverse diseases, for example, inflammation – including COVID-19 suffering from cytokine storms[22] – and lupus nephritis,[23] exploring the potential of HS/heparin-mimetics for pharmaceutical applications is raising attention. To specifically target a HS-protein interaction, it is essential to

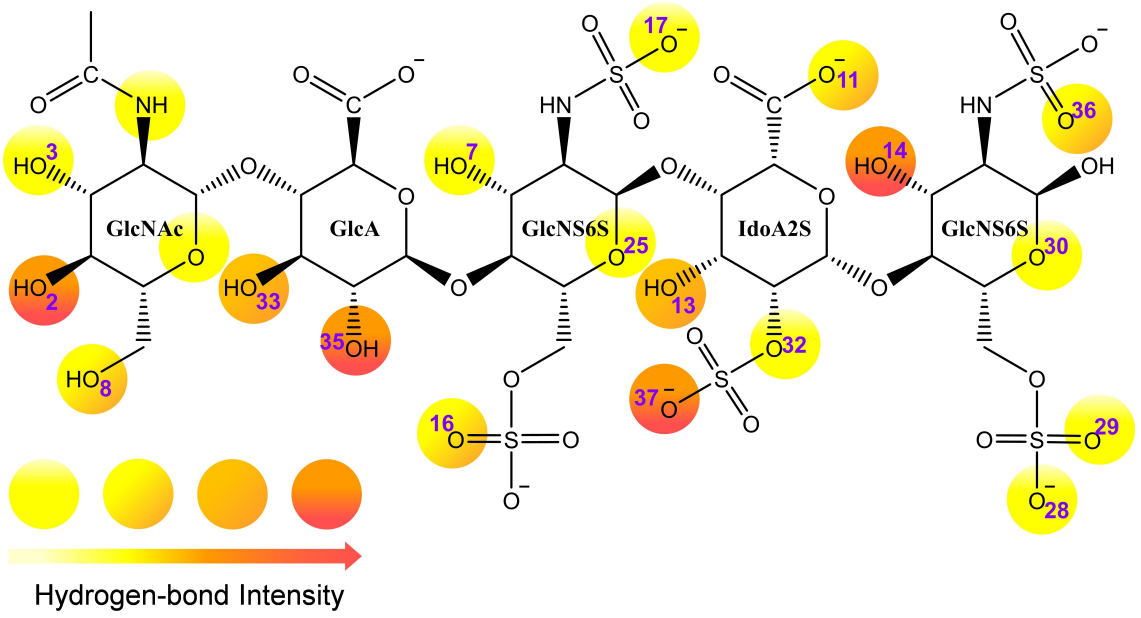

Figure 8. Cluster analysis on the frequency of the hydrogen bond interactions between heparin pentasaccharide and the 4 cytokines. The color shows intensity of hydrogen bonds. The numbers indicate the names of atoms in PDB file of heparin modeled by Chem3D 17.0 (shown in Supporting Information as Cartesian coordinates of heparin).

know the molecular structures of the target protein and the binding sequence of HS. With the increasing availability of protein structures in the PDB database discovery and rational design of specific HS-sequence through molecular modeling became more convenient. The combination of virtual screening and biochemical analysis can provide powerful tools to discover novel pharmaceutical compounds.

Experimental Section

Reagents

The cytokines used in this study include IL-2 (PeproTech, USA), IL-1beta, IL-6 and CCL8 (Sino Biological, China or PeproTach, USA). Heparin (MW≈12 kDa) was obtained from SPH No.1 Biochemical Pharmaceutical CO., LTD, China. OD-heparin (O-desulfated heparin; MW≈12 kDa), NS-K5 (N-sulfated K5 polysaccharide; MW≈60 kDa) were prepared as described,[24] HS (heparan sulfate; MW≈30 kDa) was purified from bovine lung.[25]

Preparation of Biotinylated Heparin and Immobilization

For biotinylation of heparin at the reducing end, 10 mg heparin (MW≈15 kDa, SPH No.1 Biochemical Pharmaceutical CO., LTD, #C-HEPPIM) and aniline (11 μL) in NaOAc buffer (100 mM, pH 6.0, 1.08 mL) were mixed with 120 μL of EZ-Link Alkoxyamine-PEG4-Biotin in DMSO (50 mM, Thermo Scientific #26137) and incubated at 37 °C for 48 hr. The product was purified in a 2 mL-DEAE SEPHACEL (Cytiva) column, and concentrated by ultrafiltration with a 3 kD cutoff Millipore Amicon ultrafiltration tube, followed by desalting with PD-10. Then, the lyophilized biotinylated heparin was used for the following experiment.

The streptavidin gold sensor chip was plasma cleaned prior to immobilization. The biotinylated heparin (5 μL, 2 mg ml^{-1}) was dissolved in 200 μL of HBS-P (10 mM HEPES, 150 mM NaCl, 0.005 % (v/v) surfactant P20) and immobilized onto the sensor chip with the ligand in ~800 response unit and HBS-P was used as running buffer. A multi-channel Surface Plasmon Resonance (SPR) instrument (Biacore S200, GE Healthcare) was used for the analysis. Equilibration of the baseline was performed by a continuous flow of HBS-P buffer through the chip surface for 2–4 hr between application of each protein ligand. The data were collected at 25 °C with HBS-P as running buffer at a constant flow of 30 μL min^{-1}.

Immobilization of IL-6 onto the Chips

The Series S Sensor Chip CM5 was prepared by mixing 400 mM EDC and 100 mM NHS (GE Healthcare) at a flow rate of 10 μL min^{-1} immediately prior to immobilization of the protein. IL-6 was dissolved in 10 mM NaAc (pH 4.0) to the concentration of 20 μg mL^{-1} and immobilized onto the activated sensor chip at a flow rate of 10 μL min^{-1}. The ligand density was 1050 response unit. The chip was deactivated by 1 M ethanolamine hydrochloride-NaOH at a flow rate of 10 μL min^{-1} for 420 s. A multi-channel Surface Plasmon Resonance (SPR) instrument (Biacore 8 K, GE Healthcare) was used for the analysis with 1×PBS (2 mM KH_2PO_4, 10 mM Na_2HPO_4, 137 mM NaCl, 2.7 mM KCl, pH = 7.4) as running buffer at a constant flow of 30 μL min^{-1} at 25 °C.

Surface Plasmon Resonance (SPR) Analysis

For the experiment of protein binding to immobilized heparin, the cytokines were dissolved in HBS-P buffer at the concentration of 10 mM and serially diluted with running buffer to the concentrations of 10.000, 3.333, 1.111, 0.370, 0.123, 0.041, 0.014 and 0.005 mM. The diluted samples were injected into the channel for 120 s, followed by washing of more than 360 s with the HBS-P running buffer. For the experiment of polysaccharides binding to immobilized protein, heparin, OD-heparin, NS-K5 and HS were

dissolved in 1×PBS buffer to 500 μM as start concentration that was serially diluted with running buffer to the concentrations indicated in Figure S3. The diluted samples were injected into the channel for 60 s, followed by washing more than 90 s with 1×PBS running buffer. RU was recorded to determine the binding activity of analyte. The equilibrium dissociation constant (K_D), the association {k_{on}} and dissociation {k_{off}} rate constants were determined using Equations (1) and (2) as follows.

$$dR/dt = k_{on} \times C \times (R_{max} - R) - k_{off} \times R \quad (1)$$

Here R represents the response unit and C is the concentration of the analytes.

$$K_D = k_{off}/k_{on} \quad (2)$$

Molecular Modeling of Heparin-Protein Interaction

The three-dimensional structures of IL-1beta (PDB ID: 1ITB), IL-2 (PDB ID: 6YE3), IL-6 (PDB ID: 1ALU) and CCL8 (PDB ID: 1ESR) were obtained from RCSB-PDB (www.rcsb.org). For the interaction studies, the PDB files were applied with monomers retained and cleaned with the heteroatoms (HETATM) of the receptor and ligand removed by the online CHARMM-GUI program (http://www.charmm-gui.org).[26] The PDB files of heparin and its mimetics were prepared by Chem3D 17.0.[27]

The molecular dockings of the proteins and heparin were performed by AutoDock VINA in YASARA to evaluate the binding sites and binding strength of the ligands. In brief, the proteins were maintained rigid and heparin (as ligand) was fully flexible. To remove bumps and ascertain the covalent geometry of the ligand, a pentasaccharide heparin structure was energy-minimized with the NOVA force field,[28] using the Particle Mesh Ewald algorithm[29] to treat long-range electrostatic interactions. After removal of conformational stress by a short steepest descent minimization, the procedure was continued by simulated annealing (time step 2 fs, atom velocities scaled down by 0.9 every 10th step) until convergence was reached. The blind dockings were undertaken in two steps, the former step was setting boxes of sizes 54.2 Å×54.2 Å×54.2 Å for IL-1beta, 52.16 Å×52.16 Å×52.16 Å for IL-2, 59.5 Å×59.5 Å×59.5 Å for IL-6 and 49.09 Å×49.09 Å×49.09 Å for CCL8. The latter step was docking of heparin onto each receptor protein, leading to 25 poses and 9 clusters for each situation. The binding affinity (dissociation constants, K_D values) was predicted by the calculation of free binding energy in the docking experiments.

The PQR file of IL-1beta, IL-2, IL-6 and CCL8 were generated by the online PDB2PQR server (https://server.poissonboltzmann.org/pdb2pqr) based on the molecular docking results of proteins and heparin.[30] The electrostatic potential maps of the IL-1beta, IL-2, IL-6 and CCL8 were visualized using PyMOL (version 2.3.4 by Schrödinger, LLC).

To justify whether the models constructed from molecular docking are reliable, the molecular dynamics (MD) simulations of each cytokines with a pentasaccharide heparin bound were performed. The AMBER14 force field was used for the MD simulation as implemented in the YASARA program. The MD simulation employed periodic boundary conditions, the particle-mesh Ewald method for the treatment of the long-range coulomb forces beyond a 8 Å cutoff. 0.9% NaCl (a mass fraction) was used. The cell was rescaled such that residues named HOH reach a density of 0.997 g ml^{-1}. No restraints were applied during the MD simulation using the settings employed in the second equilibration dynamics. The energies and coordinates every 100 ps were saved with a total simulation length of 400 ns at constant temperature (298 K) and pressure uncontrolled in NVT ensemble. Structural stability of the receptor-ligand complex was examined by analyzing the average values of potential energy with root mean square deviation (RMSD) throughout the trajectory. The RMSD profiles of all MD structures (Figure S1) show that the variation of the RMSD values tends to be stable (<1 Å) after 300 ns, which means that the equilibrium structures have been obtained and the last MD structures can be chosen as representative ones from the most populated cluster.

Acknowledgements

This work was supported by grants from the National Natural Science Foundation of China (31961133004), the Swedish Research Council (2018-02503, 2018-06016), the China Postdoctoral Science Foundation (2020 M670109, 2020TQ0029) and Beijing Advanced Innovation Center for Soft Matter Science and Engineering. We thank Prof. Xu-dong Qu for the support of the YASARA and Discovery studio v4.5 in molecular modeling calculation. The image of graphical abstract was created with tools obtained from BioRender.com.

Conflict of Interest

The authors declare no conflict of interest.

Keywords: heparan sulfate · heparin · inflammatory cytokine · interaction · molecular modeling

[1] S. E. Stringer, J. T. Gallagher, *Int. J. Biochem. Cell Biol.* **1997**, *29*, 709–714.
[2] a) A. J. Brown, P. R. Joseph, K. V. Sawant, K. Rajarathnam, *Int. J. Mol. Sci.* **2017**, *18*, 748; b) V. De Pasquale, L. M. Pavone, *Int. J. Mol. Sci.* **2020**, *21*, 4211.
[3] J. P. Li, M. Kusche-Gullberg, *Int. Rev. Cell Mol. Biol.* **2016**, *325*, 215–273.
[4] C. R. Parish, *Nat. Rev. Immunol.* **2006**, *6*, 633–643.
[5] C. Huang, Y. Wang, X. Li, L. Ren, J. Zhao, Y. Hu, L. Zhang, G. Fan, J. Xu, X. Gu, Z. Cheng, T. Yu, J. Xia, Y. Wei, W. Wu, X. Xie, W. Yin, H. Li, M. Liu, Y. Xiao, H. Gao, L. Guo, J. Xie, G. Wang, R. Jiang, Z. Gao, Q. Jin, J. Wang, B. Cao, *Lancet* **2020**, *395*, 497–506.
[6] M. R. Schenauer, Y. Yu, M. D. Sweeney, J. A. Leary, *J. Biol. Chem.* **2007**, *282*, 25182–25188.
[7] a) L. A. Borghesi, Y. Yamashita, P. W. Kincade, *Blood* **1999**, *93*, 140–148; b) S. Najjam, B. Mulloy, J. Theze, M. Gordon, R. Gibbs, C. C. Rider, *Glycobiology* **1998**, *8*, 509–516; c) Y. I. Oh, G. J. Sheng, S. K. Chang, L. C. Hsieh-Wilson, *Angew. Chem. Int. Ed.* **2013**, *52*, 11796–11799; *Angew. Chem.* **2013**, *125*, 12012–12015; d) S. Salek-Ardakani, J. R. Arrand, D. Shaw, M. Mackett, *Blood* **2000**, *96*, 1879–1888; e) D. Spillmann, D. Witt, U. Lindahl, *J. Biol. Chem.* **1998**, *273*, 15487–15493.
[8] H. Lortat-Jacob, *Curr. Opin. Struct. Biol.* **2009**, *19*, 543–548.
[9] C. Shi, C. Wang, H. Wang, C. Yang, F. Cai, F. Zeng, F. Cheng, Y. Liu, T. Zhou, B. Deng, I. Vlodavsky, J. P. Li, Y. Zhang, *Clin. Transl. Sci.* **2020**, *13*, 1087–1095.
[10] a) B. Casu, I. Vlodavsky, R. D. Sanderson, *Pathophysiol. Haemostasis Thromb.* **2008**, *36*, 195–203; b) B. Mulloy, *Curr. Opin. Pharmacol.* **2019**, *46*, 50–54.
[11] a) M. M. Fuster, J. D. Esko, *Nat. Rev. Cancer* **2005**, *5*, 526–542; b) R. Sasisekharan, Z. Shriver, G. Venkataraman, U. Narayanasami, *Nat. Rev. Cancer* **2002**, *2*, 521–528.
[12] M. Rusnati, A. Bugatti, S. Mitola, D. Leali, P. Bergese, L. E. Depero, M. Presta, *Sensors* **2009**, *9*, 6471–6503.

[13] a) H. Land, M. S. Humble, *Methods Mol. Biol.* **2018**, *1685*, 43–67; b) O. Trott, A. J. Olson, *J. Comput. Chem.* **2010**, *31*, 455–461.
[14] N. A. Baker, D. Sept, S. Joseph, M. J. Holst, J. A. McCammon, *Proc. Natl. Acad. Sci. USA* **2001**, *98*, 10037–10041.
[15] D. Xu, J. D. Esko, *Annu. Rev. Biochem.* **2014**, *83*, 129–157.
[16] A. Ori, M. C. Wilkinson, D. G. Fernig, *J. Biol. Chem.* **2011**, *286*, 19892–19904.
[17] S. E. Mottarella, D. Beglov, N. Beglova, M. A. Nugent, D. Kozakov, S. Vajda, *J. Chem. Inf. Model.* **2014**, *54*, 2068–2078.
[18] A. Geissner, P. H. Seeberger, *Annu. Rev. Anal. Chem.* **2016**, *9*, 223–247.
[19] F. Zhang, L. Zheng, S. Cheng, Y. Peng, L. Fu, X. Zhang, R. J. Linhardt, *Molecules* **2019**, *24*, 3360.
[20] a) S. A. Samsonov, L. Bichmann, M. T. Pisabarro, *J. Chem. Inf. Model.* **2015**, *55*, 114–124; b) A. Penk, L. Baumann, D. Huster, S. A. Samsonov, *Glycobiology* **2019**, *29*, 715–725; c) F. Zsila, S. A. Samsonov, *Carbohydr. Res.* **2018**, *462*, 28–33.
[21] W. Somers, M. Stahl, J. S. Seehra, *EMBO J.* **1997**, *16*, 989–997.
[22] F. Drago, L. Gozzo, L. Li, A. Stella, B. Cosmi, *Front. Pharmacol.* **2020**, *11*, 579886.
[23] A. L. Rops, M. J. van den Hoven, M. A. Bakker, J. F. Lensen, T. J. Wijnhoven, L. P. van den Heuvel, T. H. van Kuppevelt, J. van der Vlag, J. H. Berden, *Nephrol. Dial. Transplant.* **2007**, *22*, 1891–1902.
[24] A. Hagner-Mcwhirter, U. Lindahl, J. Li, *Biochem. J.* **2000**, *347*, 69–75.
[25] M. Maccarana, Y. Sakura, A. Tawada, K. Yoshida, U. Lindahl, *J. Biol. Chem.* **1996**, *271*, 17804–17810.
[26] S. Jo, T. Kim, V. G. Iyer, W. Im, *J. Comput. Chem.* **2008**, *29*, 1859–1865.
[27] A. Singh, D. Montgomery, X. Xue, B. L. Foley, R. J. Woods, *Glycobiology* **2019**, *29*, 515–518.
[28] E. Krieger, G. Koraimann, G. Vriend, *Proteins* **2002**, *47*, 393–402.
[29] U. P. Essmann, L. Perera, M. L. Berkowitz, T. Darden, H. Lee, L. G Pedersen, *J. Chem. Phys.* **1995**, *103*, 8577–8593.
[30] T. J. Dolinsky, J. E. Nielsen, J. A. McCammon, N. A. Baker, *Nucleic Acids Res.* **2004**, *32*, W665–667.

Manuscript received: June 7, 2021
Revised manuscript received: August 29, 2021